Acc. Sc. Torino
Memorie Sc. Fis. 38-39 (2014-2015), 23-44 MECCANICA DEI SOLIDI

On the effect of support asymmetry on rotordynamic instability

Memoria del Socio nazionale residente GIANCARLO GENTA* presentata nell'adunanza del 7 maggio 2014 e approvata nell'adunanza dell'11 giugno 2014

Riassunto. *Una delle cause di instabilità dei rotori è lo smorzamento della parte rotante del sistema, il cui effetto instabilizzante può essere combattuto solamente introducendo un sufficiente smorzamento non rotante. È ben noto che la soglia di instabilità cresce al crescere del rapporto del secondo rispetto al primo. Nel presente lavoro si dimostra che l'anisotropia dei supporti agisce in favore della stabilità innalzando la soglia di instabilità, ma solamente nel caso in cui tale anisotropia riesca a rendere ellittiche le orbite di precessione del sistema.*

Parole chiave: dinamica dei rotori, campi di instabilità, anisotropia dei supporti, smorzamento strutturale, rotore di Jeffcott.

Abstract. *One of the causes of rotor instability is the damping of the rotating parts of the system. Its de-stabilizing effect can be counteracted only by introducing a suitable non rotating damping. It is well known that the instability threshold increases at increasing ratio between non rotating and rotating damping. The aim of the present paper is showing that support anisotropy tends to increase the stability of the system, by increasing the instability threshold. This effect is however present only if this anisotropy causes the whirl orbits to become elliptical.*

Keywords: rotordynamics, instability, support anisotropy, viscous damping, hysteretic damping, Jeffcott rotor.

1. Introduction

The destabilizing role of rotating damping and the opposite stabilizing role of non rotating damping in supercritical operation of rotors is well known [1-4]. This effect is has been demonstrated for all types of rotors and for any type of damping: actually what matters is the presence of a mechanism causing energy dissipation, and whether this mechanism can be associated to the

* Accademia delle Scienze di Torino; Politecnico di Torino; e-mail: giancarlo.genta@polito.it

rotating or the non-rotating parts of the machine. Even cases which may look like contradicting these general statement, like the stabilizing effect of blade dampers on bladed disc vibration find an explanation within the same conceptual frame [4, 5].

On the other side, also the effect of anisotropy on the dynamic behaviour of rotors is well known. [1, 4, 6-8], and in particular are known the different roles played by rotating and non rotating anisotropy (or, as it is usually said, the rotor and the stator anisotropy). While rotating anisotropy strongly affects free whirling, with the possibility of causing instability, non rotating anisotropy may have a strong effect on the response to unbalance but is usually considered to have a small effect on free whirling.

While this is generally true, there are cases where the non rotating anisotropy may affect also free whirling, although in an indirect way, with a stabilizing effect in the supercritical range. This can be heuristically explained saying that in synchronous whirling rotating damping has no effect, while in the supercritical range its effect of transferring energy from rotation to vibration (de-stabilizing effect) is stronger than its usual effect of dissipating energy (stabilizing effect). This is strictly linked with the circular shape of the rotor's orbits.

If the support anisotropy causes the orbits to be elliptical, some energy is dissipated by rotating damping even in synchronous whirling conditions and in the supercritical range energy dissipation increases, thus playing in favour of stability.

The aim of the present paper is to demonstrate this using simple rotor models and to show that this is also the case for complex rotors using numerical FEM models. An example and a counter-example show the increase of stability that can occur and the limits of this effect.

2. Jeffcott rotor with viscous damping

2.1. Model definition and equations of motion

The simplest model of a rotating system is the so-called Jeffcott rotor: a point mass on a massless shaft. Since only the lateral behaviour is considered, it has two degrees of freedom.

A sketch of the Jeffcott rotor is shown in Fig. 1a, where the reference frame here used is also reported. The point mass m is located in point P, with an eccentricity ε with respect to the elasticity centre C. The polar diagram of the stiffness of a symmetric and an asymmetric support (Fig. 1b) is shown in Fig. 1c.

If all the system is isotropic (axially symmetric), with reference to Fig. 1, the equation of motion written in terms of x and y coordinates is [4]:

$$\begin{cases} m\ddot{x} + (c_n + c_r)\dot{x} + kx + \Omega c_r y = m\varepsilon\Omega^2 \cos(\Omega t) \\ m\ddot{y} + (c_n + c_r)\dot{y} + ky - \Omega c_r x = m\varepsilon\Omega^2 \sin(\Omega t) \end{cases} \tag{1}$$

This equation is so well known that no comment is required. By studying the homogenous equation associated with Eq. (1), it is possible to assess that the critical speed of the undamped system is

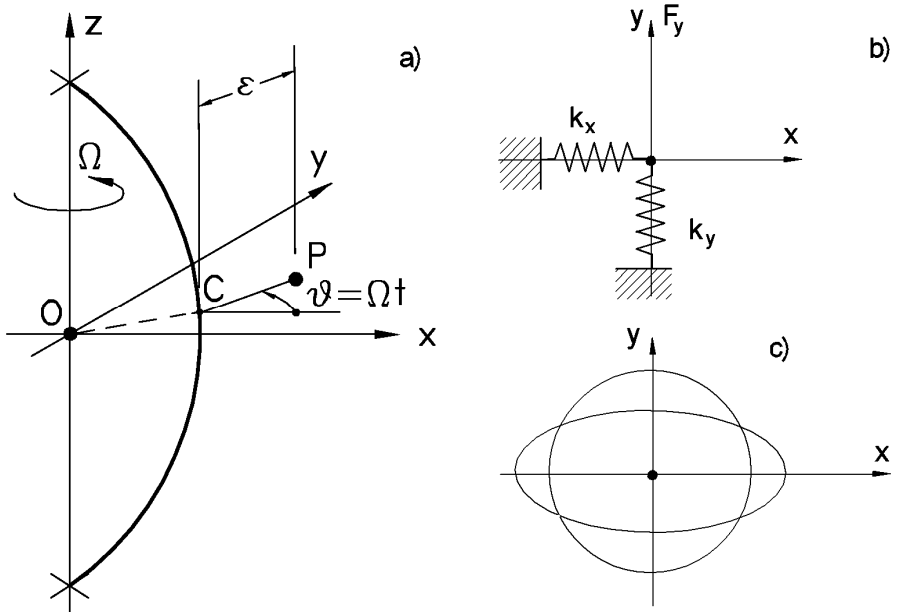

Fig. 1. Jeffcott rotor. a): Sketch of the system: the point mass *m* is located in point P, with an eccentricity ε with respect to the elasticity centre C. b) Stiffness of the supports. c) Polar diagram of the stiffness of the support for the isotropic and the non isotropic cases.

$$\Omega_{cr} = \sqrt{\frac{k}{m}} \tag{2}$$

and that the system is stable provided that the angular velocity Ω remains below a threshold of instability

$$\Omega_{th} = \sqrt{\frac{k}{m}}\left(1 + \frac{c_n}{c_r}\right) . \tag{3}$$

If the assumption of isotropy of the system is dropped, quite a different behaviour is found. As always in rotordynamics, there is much difference between the case where the lack of axial symmetry is due to the rotor or to the non-rotating parts of the system (the stator). The case where both are

non-isotropic is again different and it can be shown that no closed form solution can be found even in the simplest case of the Jeffcott rotor [4, 8]
All these cases have been extensively studied, and the attention is usually concentrated on the unbalance response in the case of isotropic rotors running on non-isotropic supports and on the free response (and consequently on the stability) when the rotor is non-isotropic but the supports have axial symmetry. Little is usually said for the stability of an isotroic rotor running on a an anisotropic stator.
This case is studied here.
The stiffness is thus considered nonisotropic and the two values k_x and k_y referred to the directions of the two axes x and y (Fig. 1b) are introduced.
Assuming that both rotating and nonrotating damping are axially symmetric, the equation of motion becomes

$$\begin{cases} m\ddot{x} + (c_n + c_r)\dot{x} + k_x x + \Omega c_r y = m\varepsilon\Omega^2 \cos(\Omega t) \\ m\ddot{y} + (c_n + c_r)\dot{y} + k_y y - \Omega c_r x = m\varepsilon\Omega^2 \sin(\Omega t) \end{cases} \tag{4}$$

The homogeneous equation of motion is written in the Laplace domain by assuming a solution of the type

$$x = x_0 e^{st}, \qquad y = y_0 e^{st}, \tag{5}$$

obtaining the following characteristic equation

$$\det\begin{bmatrix} ms^2 + (c_n + c_r)s + k_x & \Omega c_r \\ -\Omega c_r & ms^2 + (c_n + c_r)s + k_y \end{bmatrix} = 0 \ . \tag{6}$$

To reduce the number of parameters so that a simpler general discussion of the results can be done, the equation is written in nondimensional terms, where

$$s^* = s\sqrt{\frac{m}{k_{av}}}, \quad \Omega^* = \Omega\sqrt{\frac{m}{k_{av}}}, \quad \xi_n = \frac{c_n}{2\sqrt{mk_{av}}}, \tag{7}$$

$$\xi_r = \frac{c_r}{2\sqrt{mk_{av}}}, \quad \delta = \frac{k_{dev}}{k_{av}}.$$

The mean and deviatoric values of the stiffness are:

$$k_{av} = \frac{k_x + k_y}{2}, \quad k_{dev} = \frac{k_x - k_y}{2}. \tag{8}$$

Note that -1 < δ < 1.
The undamped system has now two critical speeds, which are, in nondimensional terms

$$\Omega^*_{cr\,I} = \sqrt{1 - |\delta|} \quad , \quad \Omega^*_{cr\,II} = \sqrt{1 + |\delta|} \ . \tag{9}$$

The nondimensional characteristic equation is

$$\det\begin{bmatrix} ms^{*2} + 2(\xi_n + \xi_r)s^* + 1 + \delta & 2\Omega^*\xi_r \\ -2\Omega^*\xi_r & ms^{*2} + (\xi_n + \xi_r)s^* + 1 - \delta \end{bmatrix} = 0 \ . \tag{10}$$

2.2. Eigenvalues and eigenvectors

The solutions of Eq. (10) are:

$$s^* = -(\xi_n + \xi_r) \pm \sqrt{(\xi_n + \xi_r)^2 - 1 + \sqrt{\delta^2 - 4\Omega^{*2}\xi_r^2}} \ . \tag{11}$$

The plots of the imaginary part (Campbell diagram) and of the real part (decay rate plot) of the nondimensional eigenvalues as functions of the nondimensional speed for an isotropic and an anisotropic rotor with δ = 0.4 are reported in Fig. 2.

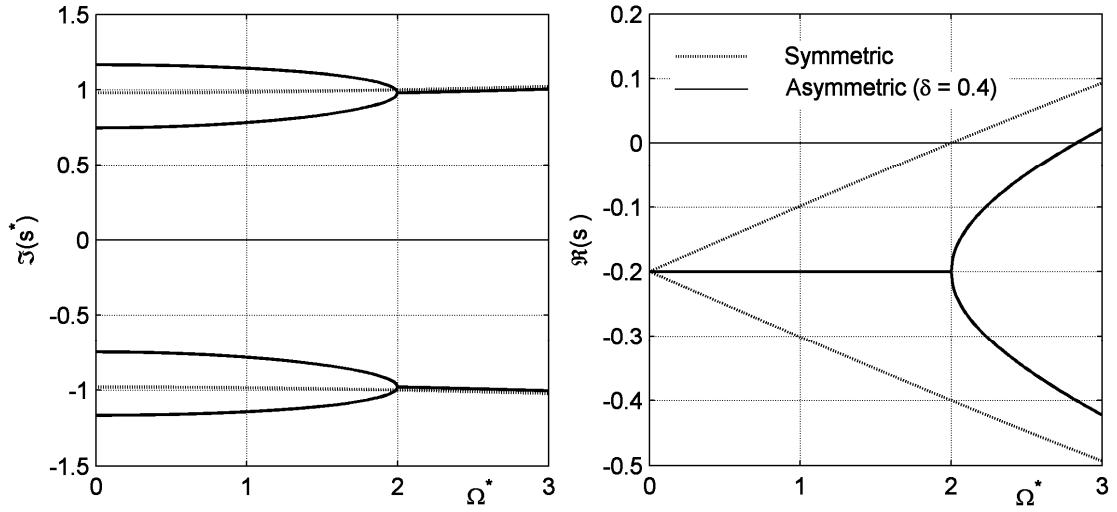

Fig. 2. Nondimensional Campbell diagram and decay rate plot for an isotropic and an anisotropic Jeffcott rotor with δ = 0.4.

Assuming that

$$\delta < 2\Omega^* \xi_r$$

the threshold of instability is

$$\Omega_{th}^* = \sqrt{\left(1 + \frac{\xi_n}{\xi_r}\right)^2 + \frac{\delta^2}{4\xi_r^2}} \quad . \tag{12}$$

It is easy to verify that if $\delta = 0$ Eq. (9) reduces to Eq. (2).
The increase of the threshold of instability with δ, i.e. with support anisotropy, can be written as

$$\frac{\Omega_{th}^*}{\left(\Omega_{th}^*\right)_{\delta=0}} = \sqrt{1 + \frac{\delta^2}{4\left(\xi_n + \xi_r\right)^2}} \tag{13}$$

The threshold of instability thus increases with increasing δ and this effect increases with decreasing damping as shown in Fig. 3.

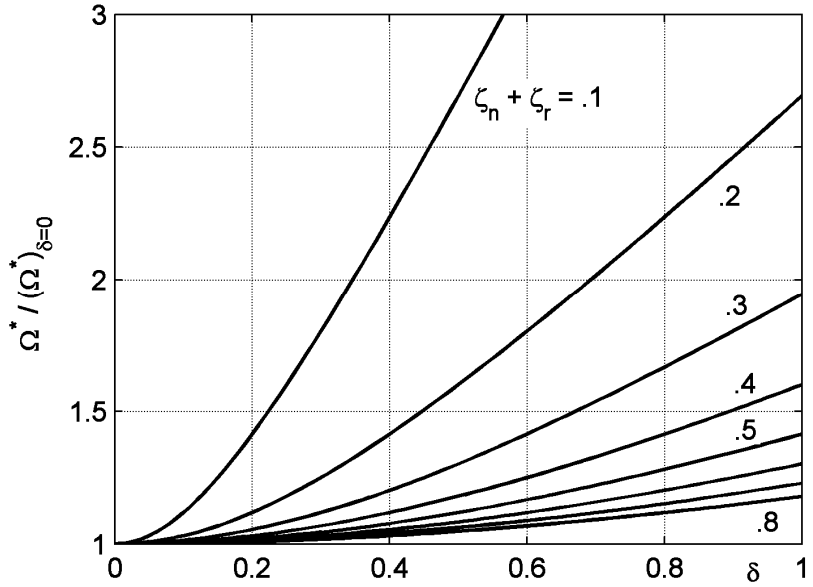

Fig. 3. Ratio between the threshold of instability of the anisotropic system and that of the isotropic one, as a function of the anisotropy parameter δ.

From the eigenvectors it is possible to compute the free whirling orbits. Those reported in Fig. 4 are related to an isotropic system ($\delta = 0$) spinning at different speeds ($\Omega^* = 0$, 1, 2 and 3) and are computed assuming two different initial conditions: the system starts with zero speed from the points $x = 1$, $y = 0$ and $x = 0$, $y = 1$.

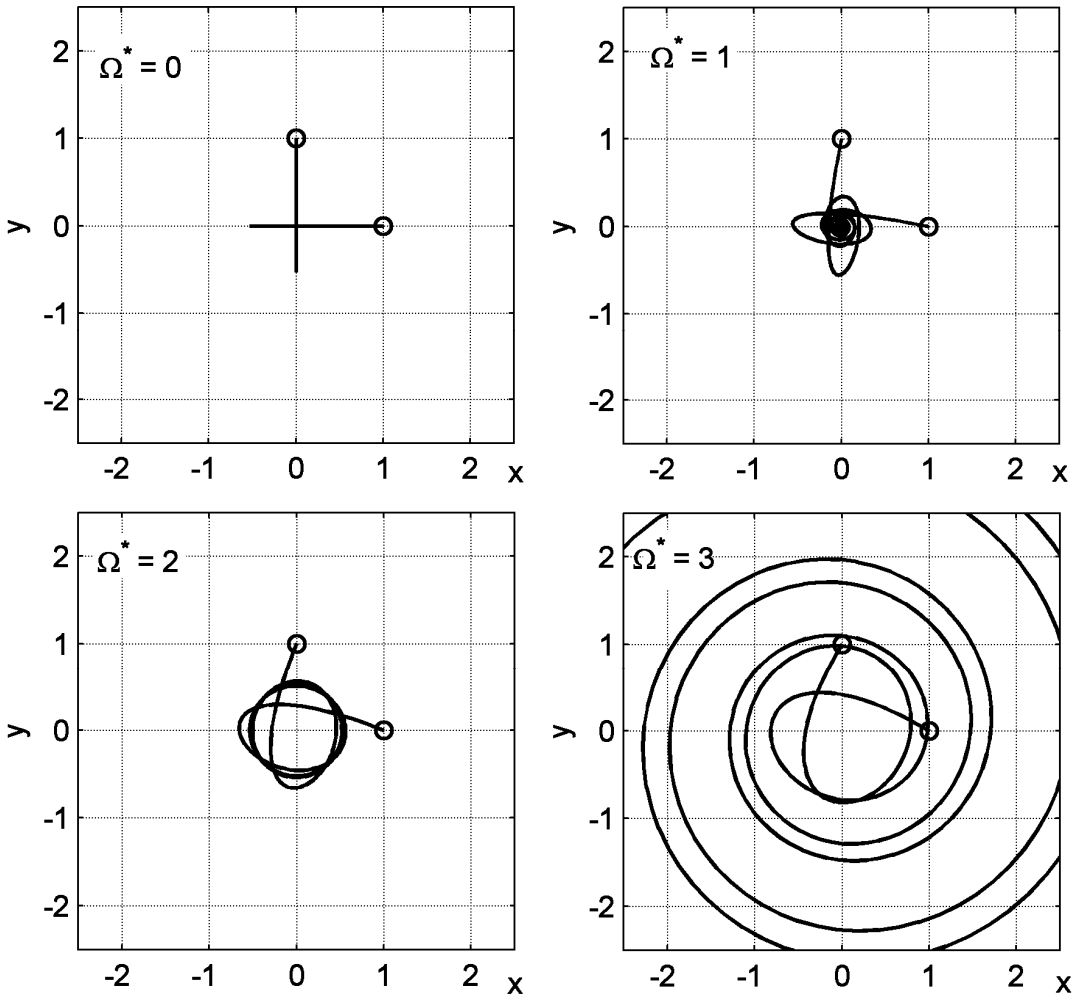

Fig. 4. Free whirling orbits for an isotropic system ($\delta = 0$) spinning at different speeds ($\Omega^* = 0$, 1, 2 and 3). Initial conditions: the system starts with zero speed from the points $x = 1$, $y = 0$ and $x = 0$, $y = 1$.

At zero speed the system oscillates in the direction of x and y axes. At $\Omega^* = 1$ the system is stable and the amplitude decays. The speed $\Omega^* = 2$ is the threshold of instability, and the amplitude neither decays or increases; owing to axial symmetry the orbits tend to be circular. At $\Omega^* = 3$ the system is unstable and the amplitude quickly grows.

The initial conditions are shown by the small circles.

The orbits reported in Fig. 5 are related to an anisotropic system ($\delta = 0.4$) spinning at different speeds ($\Omega^* = 0$, 1, 2.83 and 3) and are computed assuming the same initial conditions as before.

At zero speed the system again oscillates in the direction of x and y axes. At $\Omega^* = 1$ the system is stable and the amplitude decays. The speed $\Omega^* = 2.83$ is the threshold of instability, and the amplitude neither decays or increases; but orbits tend to be elliptical due to asymmetry. At $\Omega^* = 3$ the system is

unstable and the amplitude grows, but less quickly than before since this condition is less close to the threshold of instability.

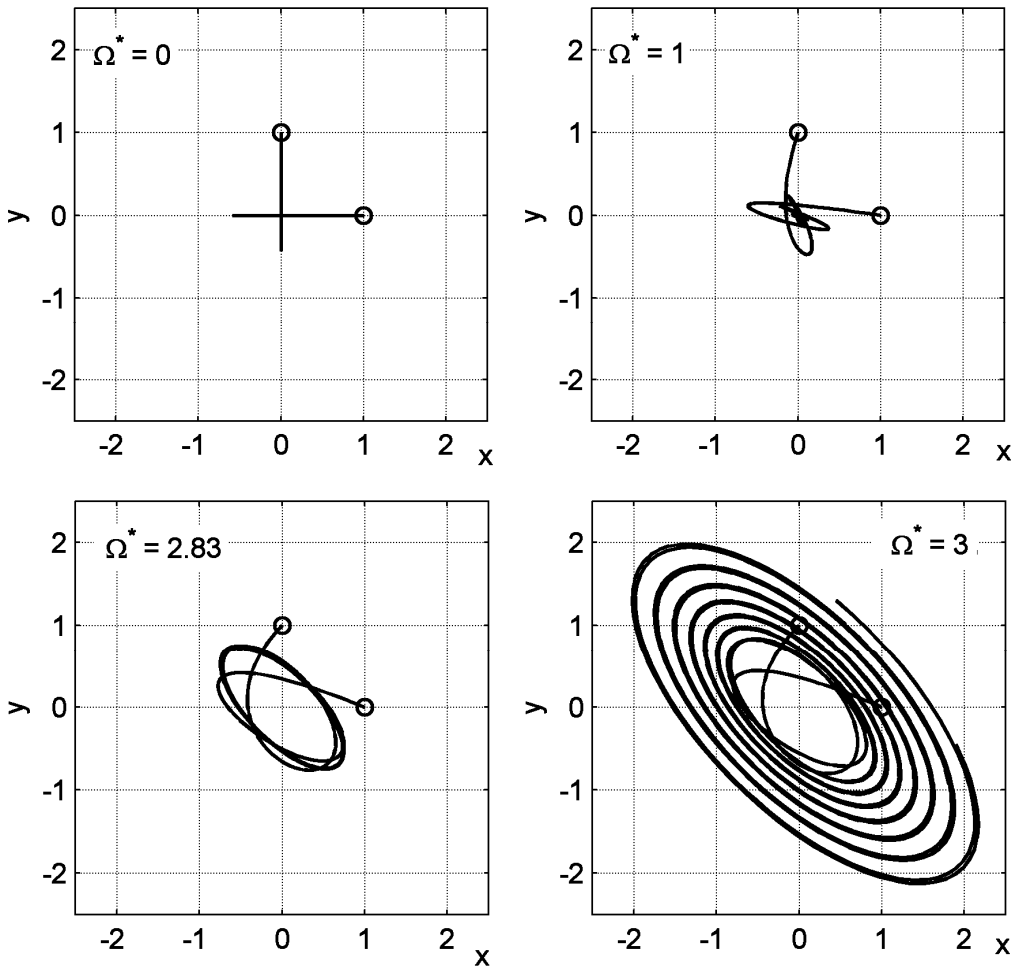

Fig. 5. Free whirling orbits for an aisotropic system ($\delta = 0.4$) spinning at different speeds ($\Omega^* = 0$, 1, 2 and 3). Initial conditions: the system starts with zero speed from the points $x = 1$, $y = 0$ and $x = 0$, $y = 1$

2.3. Considerations on the instability threshold

It is well known that in the case of isotropic systems the rotor is unstable above the critical speed if no nonrotating damping is present ($\zeta_n = 0$). The above mentioned stabilizing effect of anisotropy extends also to this case: the system can be stable above the highest critical speed

$$\Omega^*_{cr\,II} = \sqrt{1 + |\delta|}$$

provided that

$$\xi_r < \frac{|\delta|}{4}. \tag{14}$$

As already stated, an empirical explanation of this increase of stability due to anisotropy of the supports is available. If the supports are isotropic, the orbits are tendentially circular and in synchronous whirling rotating damping doesn't contribute to the energy dissipation of the system. In the supercritical range the de-stabilizing effect of rotating damping of transferring energy from the spin motion to the whirl motion becomes more is more important than the stabilizing energy dissipation effect, and the net result is a contribution to instability.

If the supports are non isotropic, on the contrary, the orbits are elliptical, and there is a motion in the rotating frame even in synchronous whirling. The energy dissipation due to rotating damping is increased, with a consequent increase of stability.

2.4. Consideration on the use of the Jeffcott rotor in the presence of rotating and nonrotating damping

The Jeffcott rotor is usually employed for assessing the roles of rotating and nonrotating damping in a simple way. However, this way of proceeding has an intrinsic flaw: rotating and nonrotating damping are assumed to act in parallel, i.e. two dampers are located between point C and point O (Fig. 1a), one of which is stationary in the Oxy frame and one rotates at speed Ω.

Although this layout may correspond to the physical situation in some particular cases [9], this is not the case in general: if both a rotating and a nonrotating damping are present, they should be associated to two different parts of the machine, a rotor and a stator, and thus they should be connected in series, and not in parallel.

3. A model with stator and rotor in series

A Jeffcott rotor with a compliant stator has been studied in [4]. A sketch of such a model is reported in Fig. 6. In the following, the stator is assumed to be unsymmetrical, and hence its stiffness and damping in x and y directions are different.

This system has 4 degrees of freedom and, assuming that the mass of the stator is negligible, its equation of motion can be written as

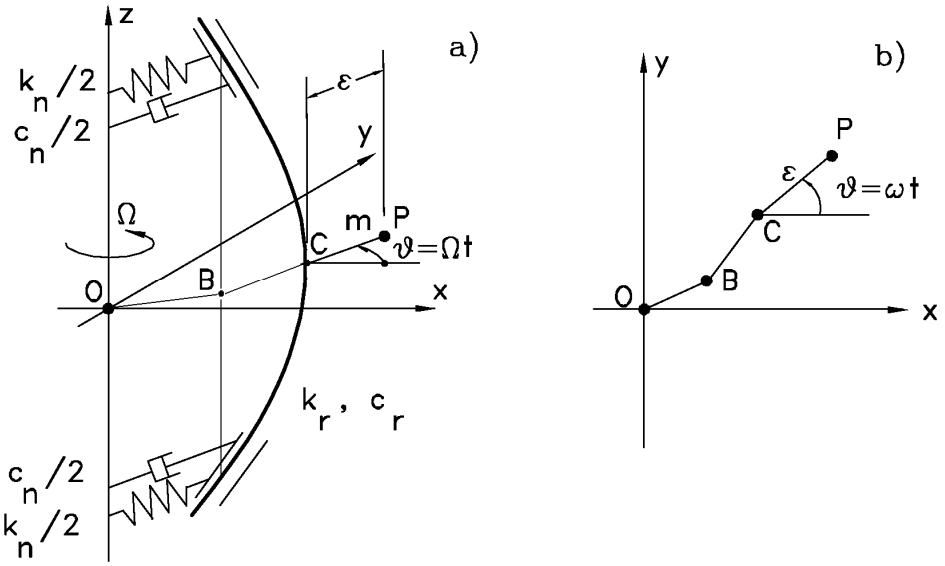

Fig. 6. Jeffcott rotor on a compliant stator. In the figure the stator is assumed to be isotropic.

$$\begin{bmatrix} m & 0 & 0 & 0 \\ 0 & m & 0 & 0 \\ 0 & 0 & 0 & 0 \\ 0 & 0 & 0 & 0 \end{bmatrix} \begin{Bmatrix} \ddot{x}_C \\ \ddot{y}_C \\ \ddot{x}_B \\ \ddot{y}_B \end{Bmatrix} + \begin{bmatrix} c_r & 0 & -c_r & 0 \\ 0 & c_r & 0 & -c_r \\ -c_r & 0 & c_r + c_{nx} & 0 \\ 0 & -c_r & 0 & c_r + c_{ny} \end{bmatrix} \begin{Bmatrix} \dot{x}_C \\ \dot{y}_C \\ \dot{x}_B \\ \dot{y}_B \end{Bmatrix} + \tag{15}$$

$$+ \left(\begin{bmatrix} k & 0 & -k & 0 \\ 0 & k & 0 & -k \\ -k & 0 & k + k_{nx} & 0 \\ 0 & -k & 0 & k + k_{ny} \end{bmatrix} + \Omega \begin{bmatrix} 0 & c_r & 0 & -c_r \\ -c_r & 0 & c_r & 0 \\ 0 & -c_r & 0 & c_r \\ c_r & 0 & -c_r & 0 \end{bmatrix} \right) \begin{Bmatrix} x_C \\ y_C \\ x_B \\ y_B \end{Bmatrix} = \begin{Bmatrix} m\varepsilon\Omega^2 \cos(\Omega t) \\ m\varepsilon\Omega^2 \sin(\Omega t) \\ 0 \\ 0 \end{Bmatrix}$$

If the system is undamped, owing to the singularity of the mass matrix, it is possible to reduce the system to an anisotropic Jeffcott rotor with mass m and stiffness

$$k_{eq_x} = \frac{k k_{nx}}{k + k_{nx}} \quad , \quad k_{eq_y} = \frac{k k_{ny}}{k + k_{ny}} \tag{16}$$

By introducing the following nondimensional parameters

$$\alpha = \frac{k_{nx} + k_{ny}}{2k} \quad , \quad \beta = \frac{c_{nx} + c_{ny}}{2c_r} \tag{17}$$

$$\delta_k = \frac{k_{nx} - k_{ny}}{k_{nx} + k_{ny}} \quad , \quad \delta_c = \frac{c_{nx} - c_{ny}}{c_{nx} - c_{ny}}$$

The equation of motion can be written in the form

$$m\begin{bmatrix} 1 & 0 & 0 & 0 \\ 0 & 1 & 0 & 0 \\ 0 & 0 & 0 & 0 \\ 0 & 0 & 0 & 0 \end{bmatrix}\begin{Bmatrix} \ddot{x}_C \\ \ddot{y}_C \\ \ddot{x}_B \\ \ddot{y}_B \end{Bmatrix} + c_r\begin{bmatrix} 1 & 0 & -1 & 0 \\ 0 & 1 & 0 & -1 \\ -1 & 0 & 1+\beta(1+\delta_c) & 0 \\ 0 & -1 & 0 & 1+\beta(1-\delta_c) \end{bmatrix}\begin{Bmatrix} \dot{x}_C \\ \dot{y}_C \\ \dot{x}_B \\ \dot{y}_B \end{Bmatrix} + \tag{18}$$

$$+\left(k\begin{bmatrix} 1 & 0 & -1 & 0 \\ 0 & 1 & 0 & -1 \\ -1 & 0 & 1+\alpha(1+\delta_k) & 0 \\ 0 & -1 & 0 & 1+\alpha(1-\delta_k) \end{bmatrix} + \Omega c_r\begin{bmatrix} 0 & 1 & 0 & -1 \\ -1 & 0 & 1 & 0 \\ 0 & -1 & 0 & 1 \\ 1 & 0 & -1 & 0 \end{bmatrix}\right)\begin{Bmatrix} x_C \\ y_C \\ x_B \\ y_B \end{Bmatrix} = \begin{Bmatrix} m\varepsilon\Omega^2\cos(\Omega t) \\ m\varepsilon\Omega^2\sin(\Omega t) \\ 0 \\ 0 \end{Bmatrix}$$

i.e.

$$m\begin{bmatrix} \mathbf{I} & \mathbf{0} \\ \mathbf{0} & \mathbf{0} \end{bmatrix}\ddot{\mathbf{X}} + c_r\begin{bmatrix} \mathbf{I} & -\mathbf{I} \\ -\mathbf{I} & \mathbf{C} \end{bmatrix}\dot{\mathbf{X}} + \left(k\begin{bmatrix} \mathbf{I} & -\mathbf{I} \\ -\mathbf{I} & \mathbf{K} \end{bmatrix} + \Omega c_r\begin{bmatrix} \mathbf{C_r} & -\mathbf{C_r} \\ -\mathbf{C_r} & \mathbf{C_r} \end{bmatrix}\right)\mathbf{X} = \mathbf{0} \tag{19}$$

where

$$\mathbf{C} = \begin{bmatrix} 1+\beta(1+\delta_c) & 0 \\ 0 & 1+\beta(1-\delta_c) \end{bmatrix}, \quad \mathbf{K} = \begin{bmatrix} 1+\alpha(1+\delta_k) & 0 \\ 0 & 1+\alpha(1-\delta_k) \end{bmatrix}, \quad \mathbf{C_r} = \begin{bmatrix} 0 & 1 \\ -1 & 0 \end{bmatrix}.$$

By introducing the nondimensional time and other quantities

$$t^* = t\sqrt{\frac{m}{k}}\sqrt{\frac{1+\alpha}{\alpha}}, \quad \Omega^* = \Omega\sqrt{\frac{m}{k}}\sqrt{\frac{1+\alpha}{\alpha}}, \quad \xi_r = \frac{c_r}{2\sqrt{mk}}\sqrt{\frac{1+\alpha}{\alpha}}, \tag{20}$$

Eq(16) can be rewritten in the form

$$\begin{bmatrix} \mathbf{I} & \mathbf{0} \\ \mathbf{0} & \mathbf{0} \end{bmatrix}\mathbf{X}'' + 2\xi_r\begin{bmatrix} \mathbf{I} & -\mathbf{I} \\ -\mathbf{I} & \mathbf{C} \end{bmatrix}\mathbf{X}' + \left(\begin{bmatrix} \mathbf{I} & -\mathbf{I} \\ -\mathbf{I} & \mathbf{K} \end{bmatrix} + 2\Omega\xi_r\begin{bmatrix} \mathbf{C_r} & -\mathbf{C_r} \\ -\mathbf{C_r} & \mathbf{C_r} \end{bmatrix}\right)\mathbf{X} = \mathbf{0} \tag{21}$$

where «and» indicate the differentiation with respect to the nondimensional time. Note that in this way the speed is made nondimensional with reference to the critical speed of the undamped isotropic rotor

Since the mass matrix is singular, it is worth while to transform the equation in the state space, which in this case has only 6 dimensions instead of 8. By introducing the state vector

$$\mathbf{z} = \begin{bmatrix} \dot{x}_C & \dot{y}_C & x_C & y_C & x_B & y_B \end{bmatrix}^T \tag{22}$$

the homogeneous equation in the state space can be written in the form

$$\begin{bmatrix} \mathbf{I} & \mathbf{0} & -2\xi_r\mathbf{I} \\ \mathbf{0} & \mathbf{0} & 2\xi_r\mathbf{C} \\ \mathbf{0} & \mathbf{I} & \mathbf{0} \end{bmatrix} \mathbf{z}'' = + \begin{bmatrix} -2\xi_r\mathbf{I} & -\mathbf{I} - 2\Omega\xi_r\mathbf{C_r} & \mathbf{I} + 2\Omega\xi_r\mathbf{C_r} \\ 2\xi_r\mathbf{I} & \mathbf{I} + 2\Omega\xi_r\mathbf{C_r} & -\mathbf{K} - 2\Omega\xi_r\mathbf{C_r} \\ \mathbf{I} & \mathbf{0} & \mathbf{0} \end{bmatrix} \mathbf{z} = \mathbf{0} \tag{23}$$

The dynamic matrix of the system is thus

$$\mathbf{A} = \begin{bmatrix} \mathbf{I} & \mathbf{0} & -2\xi_r\mathbf{I} \\ \mathbf{0} & \mathbf{0} & 2\xi_r\mathbf{C} \\ \mathbf{0} & \mathbf{I} & \mathbf{0} \end{bmatrix}^{-1} \begin{bmatrix} -2\xi_r\mathbf{I} & -\mathbf{I} - 2\Omega\xi_r\mathbf{C_r} & \mathbf{I} + 2\Omega\xi_r\mathbf{C_r} \\ 2\xi_r\mathbf{I} & \mathbf{I} + 2\Omega\xi_r\mathbf{C_r} & -\mathbf{K} - 2\Omega\xi_r\mathbf{C_r} \\ \mathbf{I} & \mathbf{0} & \mathbf{0} \end{bmatrix} \tag{24}$$

The nondimensional Campbell diagram and decay rate plot are shown in Fig. 7 in terms of the nondimensional variable

$$s^* = s\sqrt{\frac{m}{k}}\sqrt{\frac{1+\alpha}{\alpha}} \quad . \tag{25}$$

The plot had been obtained using the following values of the nondimensional variables: $\alpha = 1$, $\beta = 1$, $\delta_c = 0$, $\zeta_r = 1$ and $\delta_k = 0$ for the axysymmetric system and $\delta_k = 0.4$ for the asymmetric one.

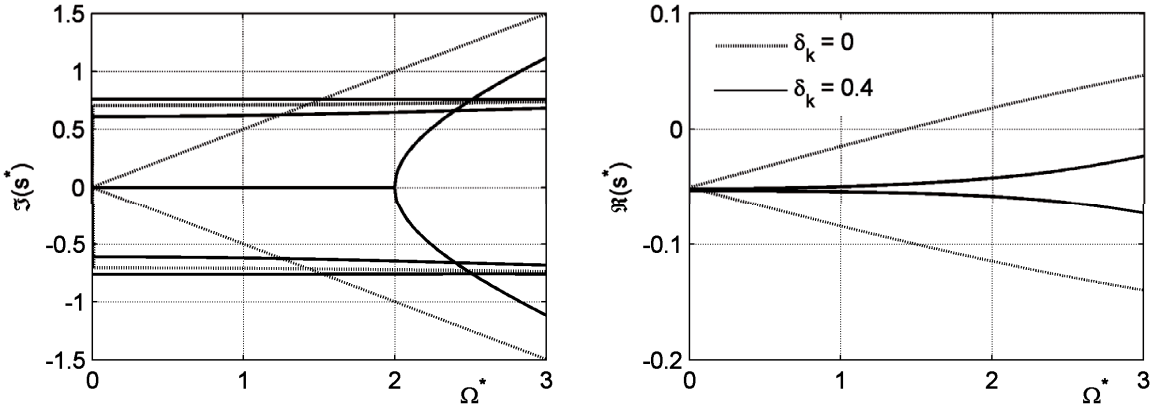

Fig. 7. Nondimensional Campbell diagram and decay rate plot for an isotropic and an anisotropic rotor with 4 degrees of freedom with $\delta = 0.4$.

The decay rate of the other modes is negative and much larger in absolute value: the modes whose decay rate is not shown are much stable and decay so fast that they have little importance in free motion.

The increase of stability due to the asymmetry is quite clear from the decay rate plot.

The free whirling orbits computed from the eigenvectors at a nondimensional speed $\Omega^* = 3$ are shown in Fig. 8 for both the isotropic system ($\delta = 0$) and the anisotropic one ($\delta = 0.4$). A single initial condition has been assumed: point C starts with zero speed from the points $x = 1$, $y = 0$.

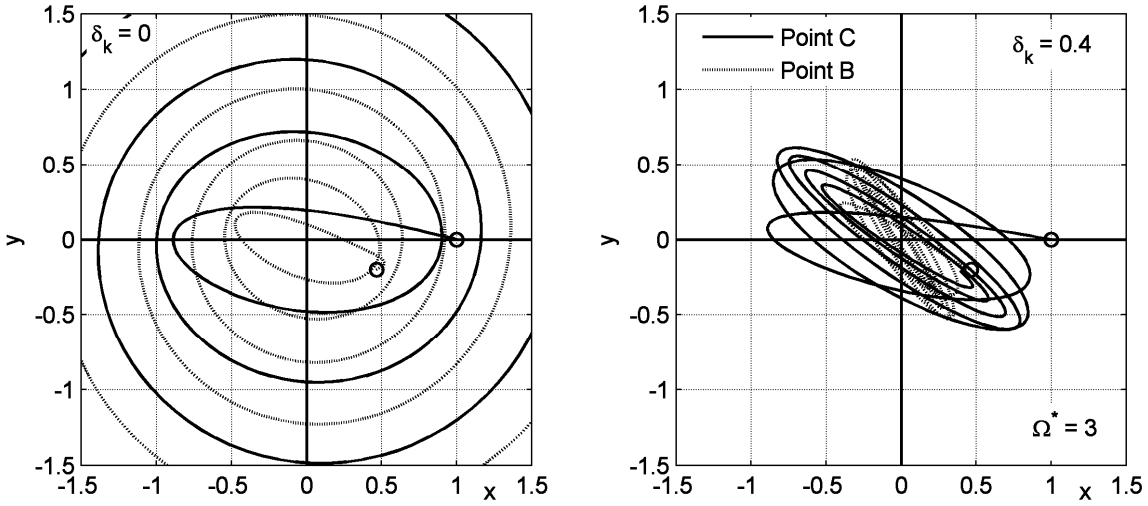

Fig. 8. Free whirling orbits for an isotropic and an anisotropic system ($\delta = 0.4$) spinning at a speed ($\Omega^* = 3$). Initial conditions: point C starts with zero speed from the points $x = 1$, $y = 0$.

4. Example: rotor of a small gas turbine

Consider the rotor of a small gas turbine sketched in Fig. 9a [10]. A finite element model, built using the DYNROT FEM code, is sketched in Fig. 9b. It consists of 10 beam and 2 mass elements. The compressor and turbine rotors can be considered rigid bodies; the stiffness of beam elements 2,3,7, and 8 is thus large (large diameter) and their mass is zero (vanishing material density) because the relevant mass is introduced as concentrated mass elements at nodes 3 and 8. The main characteristics of the elements are reported in Tab. 1 and Tab. 2.

The bearings, located at nodes 1 and 10 are modelled as anisotropic springs with stiffness

$$k_x = 70 \text{ MN/m} \quad ; \qquad k_y = 30 \text{ MN/m} .$$

The mean and deviatoric stiffness of the supports are thus

$$k_m = 50 \text{ MN/m} \quad ; \qquad k_m = 20 \text{ MN/m} \quad ; \qquad \delta = k_d / k_m = 0.4 .$$

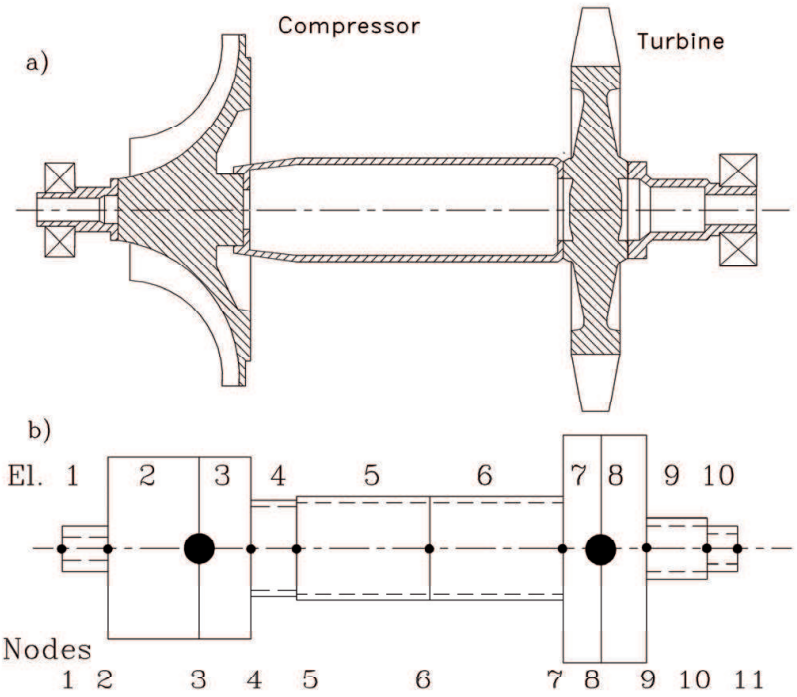

Fig. 9. Sketch and FEM model of a small gas turbine.

Tab. 1. Main characteristics of the beam elements

El. number	1	2	3	4	5	6	7	8	9	10
d_i (mm)	15	0	0	55	60	60	0	0	30	20
d_o (mm)	30	120	120	63	68	68	150	150	40	30
l (mm)	30	68.3	34.2	30	88	88	25	30	40	20
ρ (kg/m^3)	7810	0	0	7810	7810	7810	0	0	7810	7810
E (MPa)	210 000									

Tab. 2. Main characteristics of the mass elements

Element number	1	2
Node number	3	8
m (kg)	20.81	18.2
J_p (kgm^2)	0.285	0.269
J_t (kgm^2)	0.174	0.142

The first 3 critical speeds of the system with isotropic stiffness, equal to the mean stiffness, are

$$\Omega_{crI} = 1200.5 \text{ rad/s} \quad ; \quad \Omega_{crII} = 2425.0 \text{ rad/s} \quad ; \quad \Omega_{crIII} = 34031.6 \text{ rad/s} .$$

By taking into account the support anisotropy, the first 8 critical speeds are

$\Omega_{crI} = 939.9$ rad/s ; $\Omega_{crII} = 1175.6$ rad/s ; $\Omega_{crIII} = 1470.8$ rad/s
$\Omega_{crIV} = 1949.5$ rad/s ; $\Omega_{crV} = 2477.5$ rad/s ; $\Omega_{crVI} = 3551.8$ rad/s
$\Omega_{crVII} = 33625.3$ rad/s ; $\Omega_{crVIII} = 34031.5$ rad/s .

Assuming a value of the loss factor of 0.004 for the rotor and of 0.002 for the bearings, the Campbell diagram and the decay rate plot of the isotropic system are shown in Fig. 10.

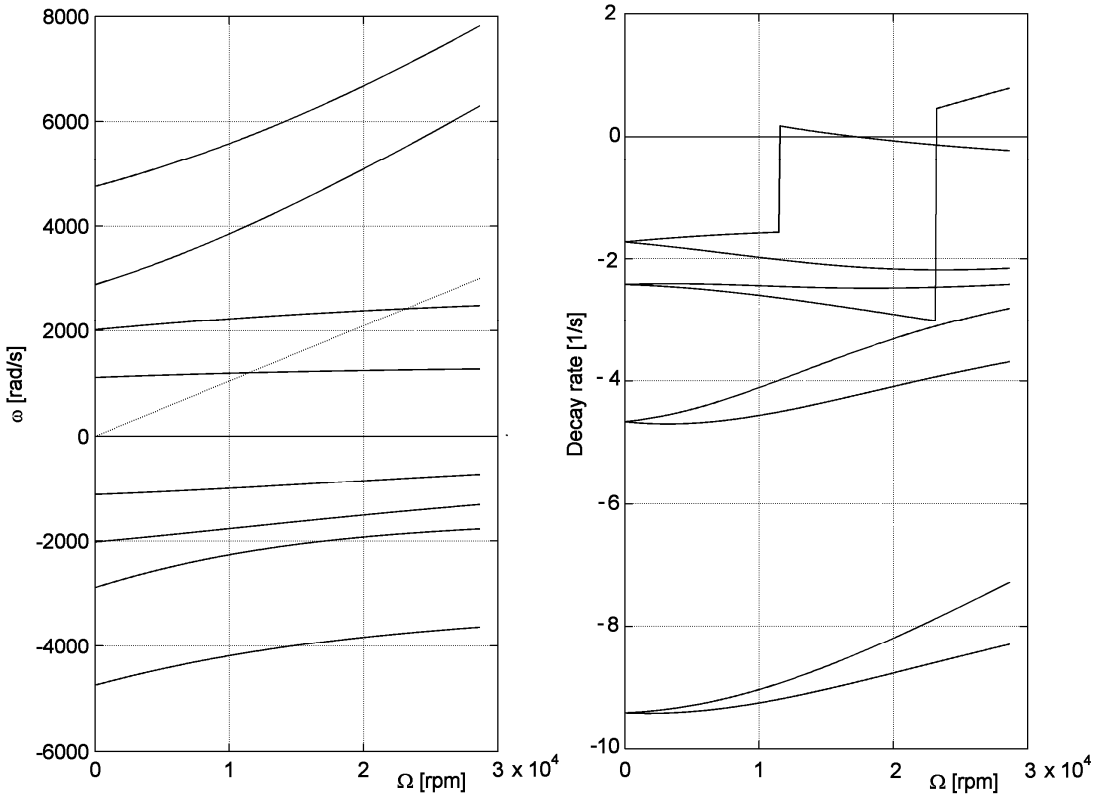

Fig. 10. Campbell diagram and decay rate plot for the small turbine of Fig. 9 running on isotropic bearings ($\delta = 0$).

As typical of rotors with hysteretic damping, the decay rate grows suddenly when crossing a critical speed, and in these cases there are two instability ranges immediately after them. The instability threshold is thus at 11540 rpm = 1209 rad/s

The Campbell diagram and the decay rate were then again computed for the case of the anisotropic bearings. The results are shown in Fig. 11.
From the plot it is clear that the decay rate has a sudden increase at about 1200 rad/s, but now it remains negative when crossing the critical speed and the system remains stable. Instability is delayed until a value of the speed close to the second critical speed of the axi-symmetric system is reached. The instability threshold is now 23680 rpm = 2480 rad/s

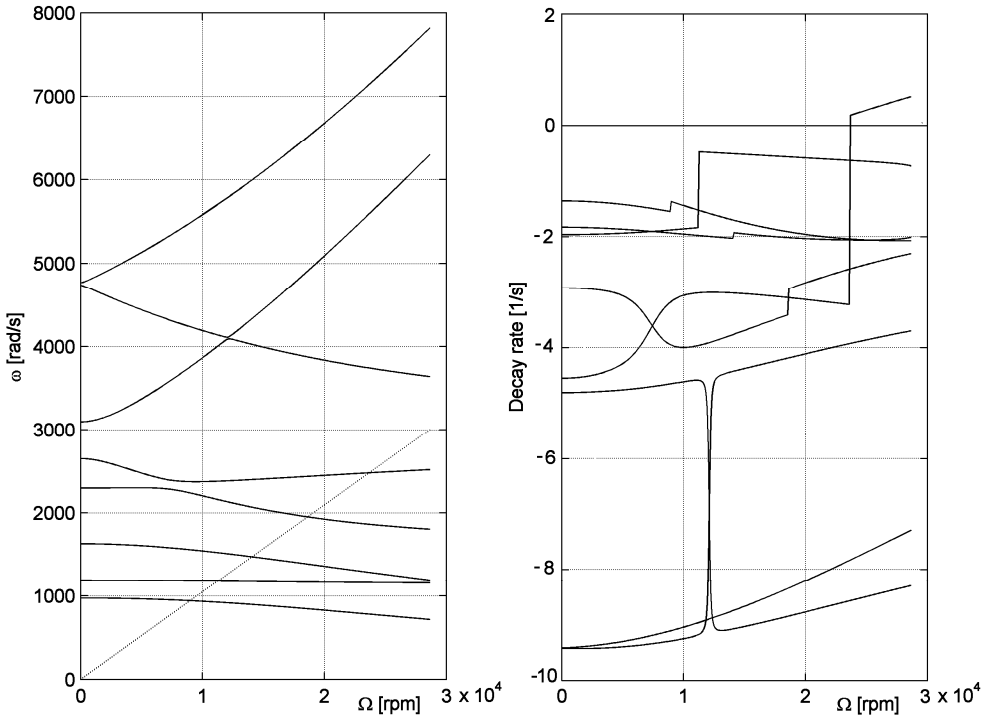

Fig. 11. Campbell diagram and decay rate plot for the small turbine of Fig. 9 running on anisotropic bearings ($\delta = 0.4$).

This example shows clearly that the stabilizing effect of the anisotropy of the bearing is present also in the case of a multi-degrees of freedom rotor with hysteretic damping.

5. Counter-example: rotor of a miniature turbojet

Consider the rotor of a miniature turbojet engine (Fig. 12a). A simple lumped parameters model is shown in Fig. 12b: it is made of 19 nodes connected with 18 Timoshenko beams elements and two concentrated masses. Two springs simulate the bearings.

The shaft between nodes 5 and 16 is modelled using beams with vanishing density and other properties coinciding the actual properties of the material (steel). The turbine wheel (between nodes 16 and 18) is modelled using two large beams, mostly for obtaining a realistic drawing, whose very large diameter coupled with the same Young's modulus of the material results in a very stiff part of the shaft.

This models reasonably well the high stiffness of this part if the rotor, caused by the presence of the wheel on the shaft. The inertial properties are introduced with a concentrated mass in node 17, whereas the density of the beam elements is set to zero. The compressor wheel is modelled in the same

way, using three massless (density equal to zero) beams, with a Young's modulus equal to that of aluminium, plus a concentrated mass. The front nut is modeled with a further beam. The properties of the beams are listed in Tab. 3, those of the mass elements in Tab. 4.

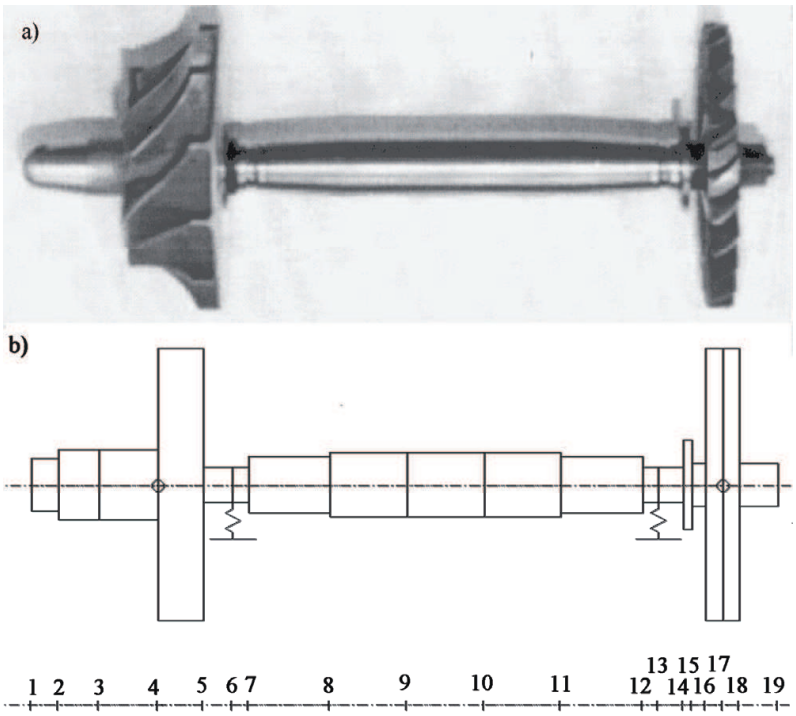

Fig. 12. Rotor of a miniature turbojet engine. a): picture of the rotor; b) sketch of the FEM model.

The bearings, located at nodes 6 and 13 are modelled as anisotropic springs with stiffness

$$k_x = 140 \text{ kN/m} \quad ; \qquad k_y = 60 \text{ kN/m} .$$

The mean and deviatoric stiffness of the supports are thus

$$k_m = 100 \text{ kN/m} \quad ; \qquad k_d = 40 \text{ kN/m} \quad ; \qquad \delta = k_d / k_m = 0.4 .$$

The first 3 critical speeds of the system with isotropic stiffness, equal to the mean stiffness, are

$$\Omega_{crI} = 802.6 \text{ rad/s} \quad ; \quad \Omega_{crII} = 866.0 \text{ rad/s} \quad ; \quad \Omega_{crIII} = 15008.0 \text{ rad/s} .$$

Tab. 3. Main characteristics of the beam elements (d: diameter; l: length; ρ: density; E: Young's modulus).

Field. #	1	2	3	4	5	6	7	8	9
d (mm)	12	16	16	60	8	8	13	14.5	14.5
l (mm)	6	9	13	10	6.5	3.5	18	17	17
ρ (kg/m$^{3)}$	7810	0	0	0	7810	7810	7810	7810	7810
E (GN/m²)	210	72	72	72	210	210	210	210	210

Field. #	10	11	12	13	14	15	16	17	18
d (mm)	14.5	13	8	8	20	10	60	60	10
l (mm)	17	18	3.5	5.5	2	3	3.8	3.7	8.5
ρ (kg/m^3)	7810	7810	7810	7810	7810	7810	0	0	7810
E (GN/m²)	210								

Tab. 4. Main characteristics of the mass elements (m: mass; J_p: polar moment of inertia; J_t: diametral moment of inertia).

Mass #	1	2
Node #	4	17
m [g]	72.1	65.8
J_p (kgm²)	2.026×10^{-5}	2.099×10^{-5}
J_t (kgm²)	1.219×10^{-5}	1.074×10^{-5}

By taking into account the support anisotropy, the first 8 critical speeds are

$$\Omega_{crI} = 602.0 \text{ rad/s} \quad ; \quad \Omega_{crII} = 670.6 \text{ rad/s} \quad ; \quad \Omega_{crIII} = 922.6 \text{ rad/s}$$
$$\Omega_{crIV} = 1023.7 \text{ rad/s} \quad ; \quad \Omega_{crV} = 7623.9 \text{ rad/s} \quad ; \quad \Omega_{crVI} = 12675.4 \text{ rad/s}$$
$$\Omega_{crVII} = 15008.0 \text{ rad/s} \quad ; \quad \Omega_{crVIII} = 30216.3 \text{ rad/s} .$$

Assuming a value of the loss factor of 0.004 for the rotor and of 0.002 for the bearings, the Campbell diagram and the decay rate plot of the isotropic system are shown in Fig. 13.

The decay rate grows suddenly when crossing a critical speed, and in these cases there is an instability range immediately after third. The instability threshold is thus at 143700 rpm = 15050 rad/s.

The Campbell diagram and the decay rate were then again computed for the case of the anisotropic bearings. The results are shown in Fig. 14.

From the plot it is clear that the anisotropy of the bearings changes little the stability of the system and the instability threshold is almost unchanged: 143200 rpm = 15000 rad/s.

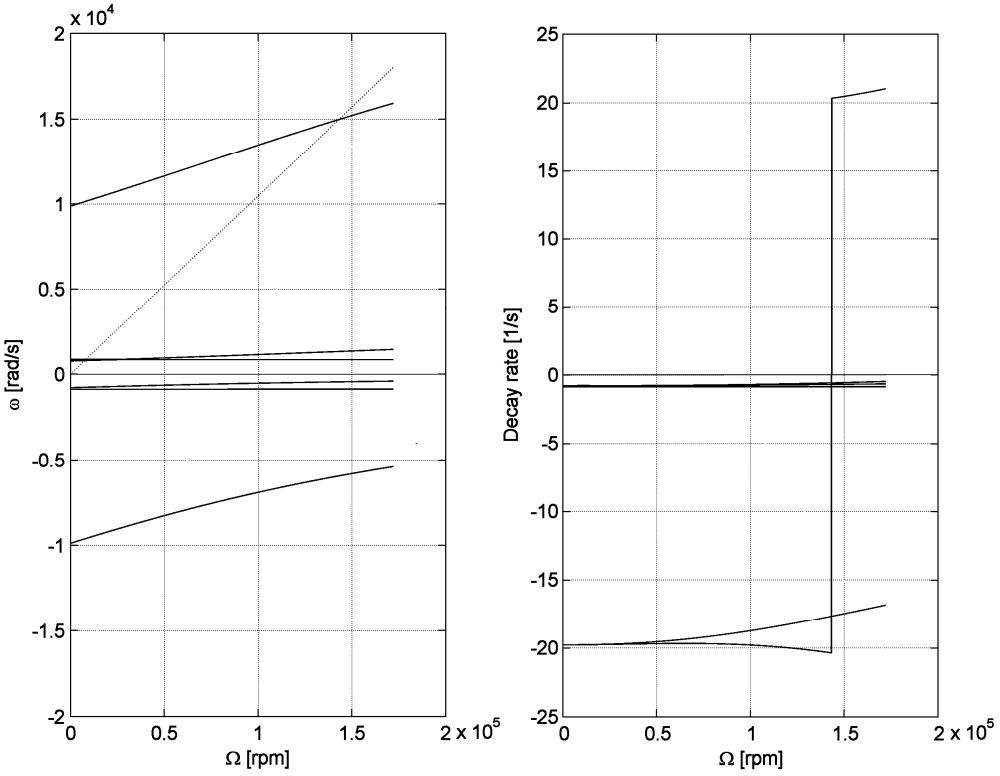

Fig. 13. Campbell diagram and decay rate plot for the miniature turbojet of Fig. 12 running on isotropic bearings ($\delta = 0$).

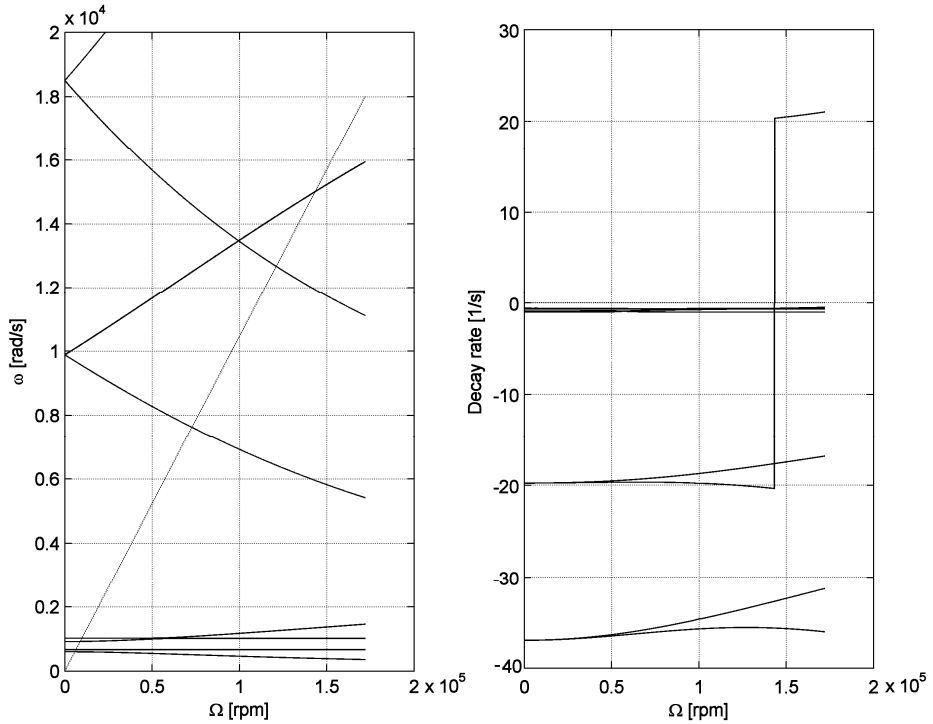

Fig. 14. Campbell diagram and decay rate plot for the miniature turbojet of Fig. 12 running on anisotropic bearings ($\delta = 0.4$).

The reason for which at the 7th critical speed (that at = 15008.0 rad/s) the bearing anisotropy is unable to stabilize the rotor becomes clear if the orbits are plotted. The mode shape has a node at node 13 (second bearing), while the orbits at the other bearing (node 6) and at the shaft mid-span (node 10) are shown in Fig. 15.
It is clear that, in spite of the anisotropy of the bearings, the orbits are circular: this example shows clearly that the stabilizing effect of the support anisotropy is strictly linked to the elliptic shape of the orbits, and that no stabilizing effect can occur if this latter feature is not present.

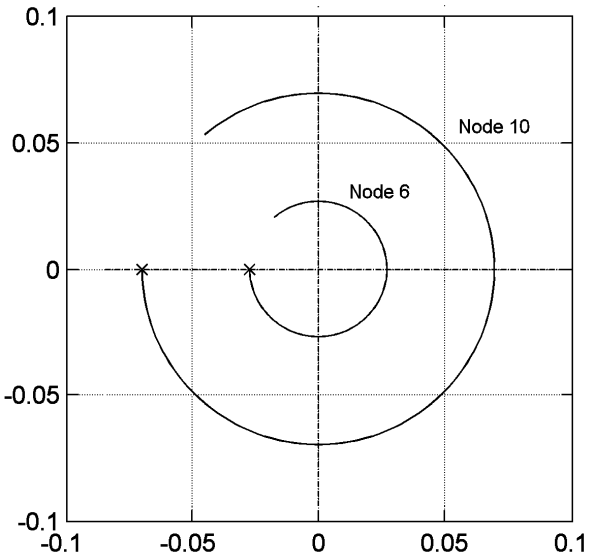

Fig. 15. Orbits at node 6 and node 10 at the 7th critical speed.

6. Conclusions

The effect of the anisotropy of the supports on the stability of a rotor with internal and external damping was studied using both highly idealized simple models and numerical FEM models of multi-d.o.f. compliant rotors.
The Jeffcott rotor is studied first, but also a more complex 4 d.o.f.s rotor is studied in which the stiffness and the damping of the the supports and the rotor are dealt with separately. This because the use of a Jeffcott rotor in which rotating and nonrotating damping are located 'in parallel' doesn't correctly model most actual situations, in which the stator and rotor elasticity and damping are located 'in series'.
As expected, the result was an increase of the threshold of instability, both in the case of viscous and hysteretic damping. An heuristic explanation of the stability increase due to support anisotropy can be given considering that anisotropic supports usually cause the orbits to be elliptical, and this orbit shape improves the energy dissipation caused by rotating damping, which in

turn makes the importance of the de-stabilizing effect of transferring energy from rotation to vibration less important.

The second example here shown confirms this simplified explanation: in a case in which the orbits remain circular in spite of the anisotropy of the supports no increase of the instability threshold was observed.

References

[1] F.M. Dimentberg, *Flexural Vibrations of Rotating Shafts*, Butterworth, London 1961.

[2] A. Tondl, *Some Problems of Rotor Dynamics*, Chapman & Hall, London 1965.

[3] R.G. Loewi and V.J. Piarulli, *Dynamics of Rotating Shafts, The Shock and Vibration Information Center*, Naval Res. Lab., Washington, D.C. 1969.

[4] G. Genta, *Dynamics of Rotating Systems*, Springer, New York 2006.

[5] G. Genta, *On the Stability of Rotating Blade Arrays*, Journal of Sound and Vibration, 273, 2004, pp. 805-836.

[6] S.H. Crandall, J. Dugundji, *Resonant Whirling of Aircraft Propeller-Engine Systems*, Journal of Applied Mechhanics, 48, 1981, pp. 929-935.

[7] S.H. Crandall, *Rotordynamics*, in W. Kliemann and N. Sri Namachchivaya (editors), *Nonlinear Dynamics and Stochastic Mechanics*, CRC Press, Boca Raton, FL 1995.

[8] G. Genta, *Whirling of Unsymmetrical Rotors, a Finite Element Approach Based on Complex Coordinates*, Journal of Sound and Vibration, 124, 1988, pp. 27-53.

[9] G. Genta, *Gyroscopic Effect and Damping in Rotordynamics*, Video included in G. Genta, *Dynamics of rotating systems*, Springer, New York 2006.

[10] G. Genta, *Vibration of Structures and Machines*, Springer, New York 2009.

Symbols

c	damping coefficient
k	stiffness
m	mass
s	Laplace variable
t	time
xyz	reference frame
δ	*Anisotropy ratio*
ε	eccentricity
ζ	damping ratio
θ	rotation angle
Ω	*spin speed*

Subscripts

av	average
cr	critical
dev	deviatoric
eq	equivalent
n	non rotating
r	rotating
th	threshold

Superscripts

*	nondimensional